First identification of rotational band structures in $^{166}_{75}Re_{91}$

H. J. Li,[1,2,*] M. Doncel,[1] M. Patial,[1] B. Cederwall,[1] T. Bäck,[1] U. Jakobsson,[1,3] K. Auranen,[3] S. Bönig,[4] M. Drummond,[5] T. Grahn,[3] P. Greenlees,[3] A. Herzáň,[3] D. T. Joss,[5] R. Julin,[3] S. Juutinen,[3] J. Konki,[3] T. Kröll,[4] M. Leino,[3] C. McPeake,[5] D. O'Donnell,[5] R. D. Page,[5] J. Pakarinen,[3] J. Partanen,[3] P. Peura,[3] P. Rahkila,[3] P. Ruotsalainen,[3,†] M. Sandzelius,[3] J. Sarén,[3] B. Sayğı,[5,‡] C. Scholey,[3] J. Sorri,[3] S. Stolze,[3] M. J. Taylor,[6] A. Thornthwaite,[5] J. Uusitalo,[3] and Z. G. Xiao[2]

[1]*Department of Physics, KTH-Royal Institute of Technology, SE-10691 Stockholm, Sweden*

[2]*Department of Physics, Tsinghua University, Beijing 100084, People's Republic of China*

[3]*University of Jyvaskyla, Department of Physics, P.O. Box 35, FI-40014 University of Jyvaskyla, Finland*

[4]*Institut für Kernphysik, TU Darmstadt, D-64289 Darmstadt, Germany*

[5]*Department of Physics, Oliver Lodge Laboratory, University of Liverpool, Liverpool L69 7ZE, United Kingdom*

[6]*School of Physics and Astronomy, University of Manchester, Manchester M13 9PL, United Kingdom*

(Received 9 March 2015; revised manuscript received 26 June 2015; published 16 July 2015)

Excited states in the odd-odd, highly neutron-deficient nucleus ^{166}Re have been investigated via the ^{92}Mo(^{78}Kr, $3p1n$)^{166}Re reaction. Prompt γ rays were detected by the JUROGAM II γ-ray spectrometer, and the recoiling fusion-evaporation products were separated by the recoil ion transport unit (RITU) gas-filled recoil separator and implanted into the Gamma Recoil Electron Alpha Tagging spectrometer located at the RITU focal plane. The tagging and coincidence techniques were applied to identify the γ-ray transitions in ^{166}Re, revealing two collective, strongly coupled rotational structures, for the first time. The more strongly populated band structure is assigned to the $\pi h_{11/2}[514]9/2^- \otimes \nu i_{13/2}[660]1/2^+$ Nilsson configuration, while the weaker structure is assigned to be built on a two-quasiparticle state of mixed $\pi h_{11/2}[514]9/2^- \otimes \nu[h_{9/2}f_{7/2}]3/2^-$ character. The configuration assignments are based on the electromagnetic characteristics and rotational properties, in comparison with predictions from total Routhian surface and particle-rotor model calculations.

DOI: 10.1103/PhysRevC.92.014310 PACS number(s): 21.10.Re, 23.20.Lv, 25.70.Jj, 27.70.+q

I. INTRODUCTION

Recent studies of the odd-odd nuclides in the $Z \approx 70$, $A \approx 160$–170 region of the Segrè chart have revealed structural effects presumably originating from the complex interplay between the odd valence neutron and proton, as well as with the deformation-soft "core." Many of these neutron-deficient nuclei are predicted by theory to be deformed in their ground states, with near-prolate shapes at $\beta_2 \approx 0.2$ [1]. Here the proton Fermi surface is near the $h_{11/2}$ subshell, influencing the electromagnetic properties of the collective rotational bands in odd-Z nuclides. The proton $h_{11/2}[514]9/2^-$ orbital is occupied in the yrast bands of rhenium nuclei in this region, which strengthens the in-band $\Delta I = 1$ transitions as a result of the high K value and large g factor for deformed configurations built on this proton orbital. The neutron Fermi surface lies near the $i_{13/2}$ orbital, which influences the rotational alignments in many nuclei in this region. For example, the first $i_{13/2}$ (AB) rotational alignment is responsible for the backbending in ^{164,166}W [2,3] and ^{163}Ta [4] and their heavier isotopes. This crossing is blocked in nearby odd-N tantalum, tungsten, and rhenium nuclei, but the next available $i_{13/2}$ crossing is an important feature in their collective structures, such as the second $i_{13/2}$ (BC) alignment in ^{165}W [3], ^{162,164,166}Ta [5–7], and ^{170,172}Re [8,9]. The occupation of the proton $h_{11/2}$ and neutron $i_{13/2}$ intruder orbitals near the Fermi level may also lead to shape polarization effects, particularly in the γ degree of freedom, owing to the spatial orientation of these orbitals [10]. An experimental indicator of a triaxial shape in odd-A nuclei is the presence and magnitude of signature splitting in the rotating frame between the energies of states belonging to different signature quantum numbers. Some nuclei in this region, in particular odd-odd nuclei, are also known to exhibit an anomalous signature splitting, or even signature inversion [6,9,11,12], a phenomenon for which there is still no consistent theoretical explanation.

The nuclide ^{166}Re is situated 19 neutrons away from the line of β stability. Spectroscopic studies of excited states in such highly neutron-deficient isotopes in the $A \approx 160$–170 mass region are experimentally highly challenging as the production cross sections in fusion-evaporation reactions decrease steeply as a function of the distance from the line of stability and a high γ-ray background originating from the fission events is present. Hence, the observation of excited states requires effective suppression of fission events, e.g., by using a recoil separator to select the fusion-evaporation residues, or even more selective techniques, such as the recoil-decay tagging technique [13,14].

Excited states in ^{166}Re were first reported in a study of the α-decay properties of ^{170}Ir and several γ-ray transitions were identified [15]. Here we report the first observation of high-spin states in ^{166}Re and the presence of two rotational structures. This work makes the nucleus ^{166}Re the lightest odd-odd rhenium isotope that has been reported to date to exhibit collective rotational excitations.

*hongjiel@kth.se

†Current address: TRIUMF, 4004 Wesbrook Mall, Vancouver, British Columbia, Canada V6T 2A3.

‡Current address: Department of Physics, Faculty of Science, Ege University, 35100 Bornova, Izmir, Turkey.

II. EXPERIMENT AND RESULTS

Excited states of ^{166}Re were populated by means of the ^{92}Mo(^{78}Kr, $3p1n$)^{166}Re fusion-evaporation reaction at a bombarding energy of 380 MeV. The experiment was conducted at the accelerator laboratory of the University of Jyväskylä, Finland. A 0.6 mg/cm^2 thick ^{92}Mo target was bombarded by the ^{78}Kr beam provided by the K-130 cyclotron. The experiment was designed primarily for lifetime measurements of excited states in ^{166}Os using the Differential Plunger for Unbound Nuclear States device [16]. A 1 mg/cm^2 Mg degrader foil was applied to slow the recoils from $v/c = 0.044$ to $v/c = 0.034$ and was placed at nine different distances from 5 to 8000 μm downstream from the target position. The prompt γ rays were detected by the γ-ray spectrometer situated at the Department of Physics, University of Jyväskylä, Finland (JUROGAM II) array, which consists of 15 EUROGAM Phase-I [17] and GASP-type [18] germanium detectors in two rings with 5 detectors at 157.6° and 10 at 133.6°, and 24 clovers [19] in two rings with 12 at 104.5° and the other 12 at 75.5° relative to the beam direction. The gas-filled recoil separator RITU (recoil ion transport unit) [20–22] was used to separate the fusion-evaporation products from the beam particles and fission products. The separated reaction products and any subsequent proton and α decays were detected by two double-sided silicon strip detectors (DSSSDs) [23] at the focal plane of RITU. The flight time of recoiling fusion-evaporation products through RITU is well defined (in the present experiment around 0.5 μs). This was used to select prompt coincidences between γ rays detected in JUROGAM II when followed by subsequent detection of recoils in the DSSSDs. The data were recorded by the triggerless total data readout (TDR) acquisition system [24]. The on- and off-line data were sorted using the GRAIN [25] software package.

A γ-γ-γ coincidence cube and several γ-γ coincidence symmetric matrices were constructed for the coincidence analysis of prompt γ rays detected with the requirement of a subsequent fusion-evaporation residue detected at the focal plane of RITU. Two asymmetric matrices with γ-ray energies detected in the clover detectors on one axis and γ-ray energies detected in the other detectors on the other axis were also constructed for measuring the multipolarities of the γ-ray transitions. The cube and the matrices were analyzed using the RADWARE software package [26]. The results of the lifetime measurements for excited states in ^{166}Re and their theoretical interpretation will be reported elsewhere [27].

The resulting level scheme for ^{166}Re is shown in Fig. 1. It was built based on the coincidence information between γ rays and rhenium x rays, coincidences with the γ-ray transitions identified in Ref. [15], as well as the DCO ratios. Two collective bands labeled with numbers (1) and (2) are identified for the first time in the present work. The state (6^+) is tentatively placed at an unknown excitation energy, X2, as we cannot exclude that there is an unobserved low-energy transition connecting it to the lower-lying state which is depopulated by the 110- and 176-keV γ-ray transitions. Typical γ-ray coincidence spectra are shown in Figs. 2 and 3 for bands (1) and (2), respectively. The spectral quality is affected by the use of a plunger device for detector angles

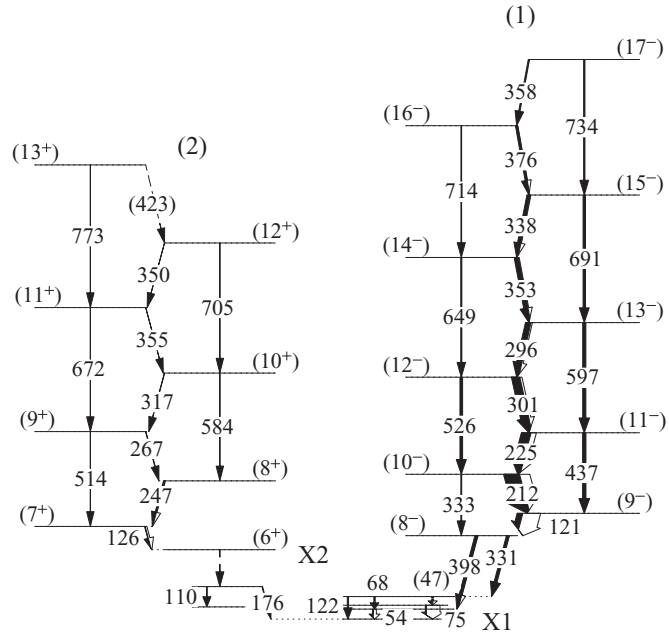

FIG. 1. The level scheme of ^{166}Re deduced from the present work. The energy is in keV. The states and γ-ray transitions below (6^+) have been described in Ref. [15].

differing from 90° relative to the beam axis. Accurate energy determinations for the observed γ-rays could be obtained for all target-degrader distances from the clover detectors, which were placed close to the plane extending from the target perpendicular to the beam axis. This is illustrated in Figs. 2 and 3. Figure 2(a) is produced by gating on the 121-keV γ-ray transition from the clover data. Figure 2(b) shows a gate on the 225-keV γ-ray transition from data collected at the target-degrader distances between 1000 and 8000 μm, where the fully Doppler-shifted line component emitted before the degrader is dominant for the states above (8^-). Figure 2(c) presents a spectrum obtained from the triple-coincidence cube, where two double gates on the 212/225- and 301/296-keV γ-ray transition pairs are added. Figure 3(a) is obtained by gating on the 126-keV γ-ray transition in band (2) from the matrix containing only the clover data. Figure 3(b) presents the 267-keV gate using the data taken at target-degrader distances between 1000 and 8000 μm, where the component emitted before the degrader dominates completely. The peaks marked with stars in Fig. 3 correspond to transitions in band (1), suggesting some unidentified linking transitions between these two bands. A summary of γ-ray energies, relative intensities (normalized to the 121-keV transition), DCO ratios, multipolarities, spin and parity assignments, as well as the corresponding level energies of ^{166}Re is given in Table I. The DCO ratios are defined as

$$R_{\mathrm{DCO}} = \frac{I_{\gamma_1}^{\theta_1}(\text{gate on } \gamma_2 \text{ at } \theta_2)}{I_{\gamma_1}^{\theta_2}(\text{gate on } \gamma_2 \text{ at } \theta_1)}. \quad (1)$$

θ_1 means the clover detectors while θ_2 represents the other detectors. The DCO ratios were obtained by gating on γ-ray transitions assigned to be of stretched dipole character. If the

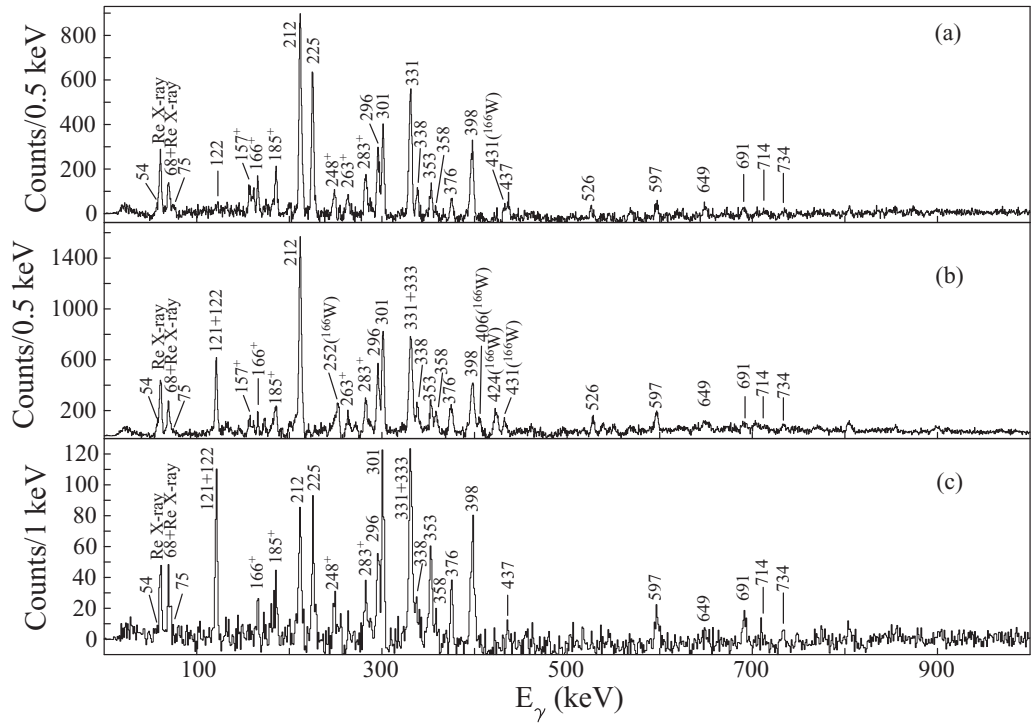

FIG. 2. (a) γ-ray energy coincidence spectrum obtained from gating on the 121-keV γ-ray transition in band (1) from the clover data. (b) γ-ray energy coincidence spectrum obtained from a gate on the 225-keV γ-ray transition in band (1) taken at target-degrader distances from 1000 to 8000 μm. (c) Spectrum obtained from the triple-coincidence cube using a sum of double gates on the 212/225-keV and 301/296-keV γ-ray transition pairs in band (1). +, γ-ray transitions not assigned in the level scheme in Fig. 1.

ratio is around 1, a stretched dipole transition is expected while a stretched $E2$ transition will be assigned when $R_{\rm DCO}$ is about 0.5.

III. DISCUSSION

Pairing self-consistent Woods-Saxon-Strutinsky type calculations using the total Routhian surface (TRS) approach

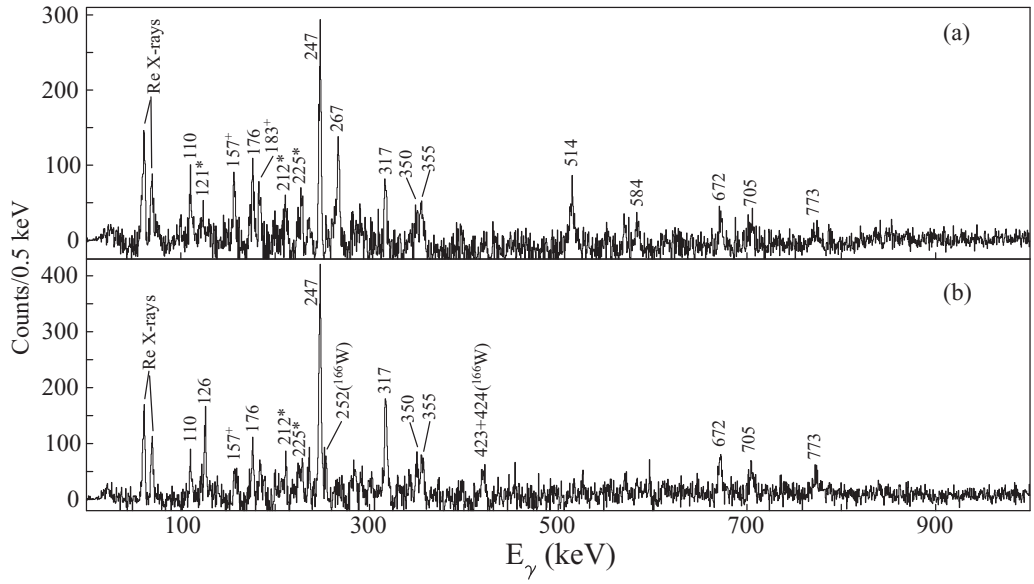

FIG. 3. (a) γ-ray energy coincidence spectrum from the clover detectors obtained by gating on the 126 keV γ-ray transition in band (2). (b) γ-ray energy coincidence spectrum obtained from a gate on the 267-keV γ-ray transition in band (2) taken at target-degrader distances from 1000 to 8000 μm. +, γ-ray transitions not assigned in the level scheme in Fig. 1. The peaks marked with stars are corresponding to transitions in band (1).

TABLE I. The energies, relative intensities, DCO ratios, multipolarities, and spin-parity assignments for the γ-ray transitions and levels in ^{166}Re. X1 and X2 represent the lowest state and the bandhead of band (2) in Fig. 1, respectively.

E_γ (keV)	Intensity (%)	E_i (keV)	E_f (keV)	Assignments	$R_{\rm DCO}$	Multipolarity
47(1)		X1 + 122	X1 + 75			
54(1)		X1 + 54	X1			$(E1)$[a]
68(1)		X1 + 122	X1 + 54			$(M1)$[a]
75(1)		X1 + 75	X1			$(M1)$[a]
110.0(5)	5.1(2)	X1 + 176	X1 + 66		0.8(2)	$(E1)$[a]
120.7(2)[b]	100	X1 + 573	X1 + 452	$(9^-) \rightarrow (8^-)$	1.0(1)	$(M1/E2)$
122.3(5)		X1 + 122	X1			$(E1)$[a]
125.7(3)[b]	11.0(3)	X2 + 126	X2	$(7^+) \rightarrow (6^+)$	1.3(1)	$(M1/E2)$
157(1)[c]						
166(1)[c]						
176.3(8)	4.3(2)	X1 + 176	X1			$(E1)$[a]
183(1)[c]						
185(1)[c]						
211.5(2)[b]	280(17)	X1 + 785	X1 + 573	$(10^-) \rightarrow (9^-)$	1.0(1)	$(M1/E2)$
224.8(2)[b]	173(9)	X1 + 1010	X1 + 785	$(11^-) \rightarrow (10^-)$	0.9(1)	$(M1/E2)$
247.1(3)[b]	18(3)	X2 + 373	X2 + 126	$(8^+) \rightarrow (7^+)$	0.8(1)	$(M1/E2)$
248(1)[c]						
263(1)[c]						
266.6(3)[b]	6.2(7)	X2 + 640	X2 + 373	$(9^+) \rightarrow (8^+)$	0.9(1)	$(M1/E2)$
283(1)[c]						
295.6(2)[b]	98(5)	X1 + 1607	X1 + 1311	$(13^-) \rightarrow (12^-)$	1.0(1)	$(M1/E2)$
300.8(2)[b]	146(6)	X1 + 1311	X1 + 1010	$(12^-) \rightarrow (11^-)$	0.9(1)	$(M1/E2)$
316.8(4)[b]	4.7(5)	X2 + 957	X2 + 640	$(10^+) \rightarrow (9^+)$	0.9(1)	$(M1/E2)$
330.7(2)[b]	52(4)	X1 + 452	X1 + 122		0.9(2)	
332.8(5)[b]		X1 + 785	X1 + 452			$(E2)$
337.8(3)[b]	61(5)	X1 + 2298	X1 + 1960	$(15^-) \rightarrow (14^-)$	0.9(1)	$(M1/E2)$
350.0(6)[b]	2.4(4)	X2 + 1662	X2 + 1312	$(12^+) \rightarrow (11^+)$		$(M1/E2)$
352.6(3)[b]	78(6)	X1 + 1960	X1 + 1607	$(14^-) \rightarrow (13^-)$	1.1(1)	$(M1/E2)$
354.8(5)[b]	4.1(5)	X2 + 1312	X2 + 957	$(11^+) \rightarrow (10^+)$		$(M1/E2)$
358.4(5)[b]	21(3)	X1 + 3032	X1 + 2674	$(17^-) \rightarrow (16^-)$		$(M1/E2)$
375.6(4)[b]	38(5)	X1 + 2674	X1 + 2298	$(16^-) \rightarrow (15^-)$	1.2(2)	$(M1/E2)$
397.7(2)[b]	49(4)	X1 + 452	X1 + 54		0.9(1)	
423(1)[b]		X2 + 2085	X2 + 1662	$(13^+) \rightarrow (12^+)$		$(M1/E2)$
436.6(8)[b]	58(5)	X1 + 1010	X1 + 573	$(11^-) \rightarrow (9^-)$	0.4(1)	$(E2)$
513.8(9)[b]	3.6(5)	X2 + 640	X2 + 126	$(9^+) \rightarrow (7^+)$	0.7(1)	$(E2)$
526.0(7)[b]	48(5)	X1 + 1311	X1 + 785	$(12^-) \rightarrow (10^-)$	0.7(1)	$(E2)$
583.5(8)[b]	3.7(6)	X2 + 957	X2 + 373	$(10^+) \rightarrow (8^+)$	0.8(1)	$(E2)$
596.6(5)[b]	56(4)	X1 + 1607	X1 + 1010	$(13^-) \rightarrow (11^-)$	0.8(1)	$(E2)$
648.8(8)[b]	19(3)	X1 + 1960	X1 + 1311	$(14^-) \rightarrow (12^-)$	0.6(1)	$(E2)$
672(1)[b]	1.6(5)	X2 + 1312	X2 + 640	$(11^+) \rightarrow (9^+)$	0.7(1)	$(E2)$
691(1)[b]	43(7)	X1 + 2298	X1 + 1607	$(15^-) \rightarrow (13^-)$	0.6(1)	$(E2)$
705(1)[b]	3.7(6)	X2 + 1662	X2 + 957	$(12^+) \rightarrow (10^+)$	0.8(1)	$(E2)$
714(1)[b]	12(3)	X1 + 2674	X1 + 1960	$(16^-) \rightarrow (14^-)$	0.4(1)	$(E2)$
734(1)[b]	23(5)	X1 + 3032	X1 + 2298	$(17^-) \rightarrow (15^-)$	0.5(1)	$(E2)$
773(1)[b]	2.2(5)	X2 + 2085	X2 + 1312	$(13^+) \rightarrow (11^+)$		$(E2)$

[a]The multipolarities taken from Ref. [15].
[b]The γ rays newly identified in the present work.
[c]The γ rays not assigned in the level scheme in Fig. 1.

[28,29] have been performed for different intrinsic configurations in ^{166}Re. The resulting TRSs show, for different rotational frequencies, the total energy in the rotating frame (Routhian) as a function of the deformation parameters β_2, β_4, and γ. Results corresponding to the yrast and near-yrast configurations are shown in Fig. 4. The TRS calculations produce well-developed minima with deformation parameters ($\beta_2 \approx 0.17$, $\gamma \approx 0^\circ$–8°) for the yrast band [band (1)], as shown in the top row in Fig. 4. The yrast rotational structure, up to $\hbar\omega \approx 0.40$ MeV, is predicted to be based on the $\pi h_{11/2}[514]9/2^- \otimes \nu i_{13/2}[660]1/2^+$ Nilsson configuration. When the rotational frequency increases from the bandhead at $\hbar\omega \approx 0.15$ MeV, the quadrupole deformation parameter stays constant at $\beta_2 \approx 0.17$, while the γ-deformation parameter changes from a slightly positive

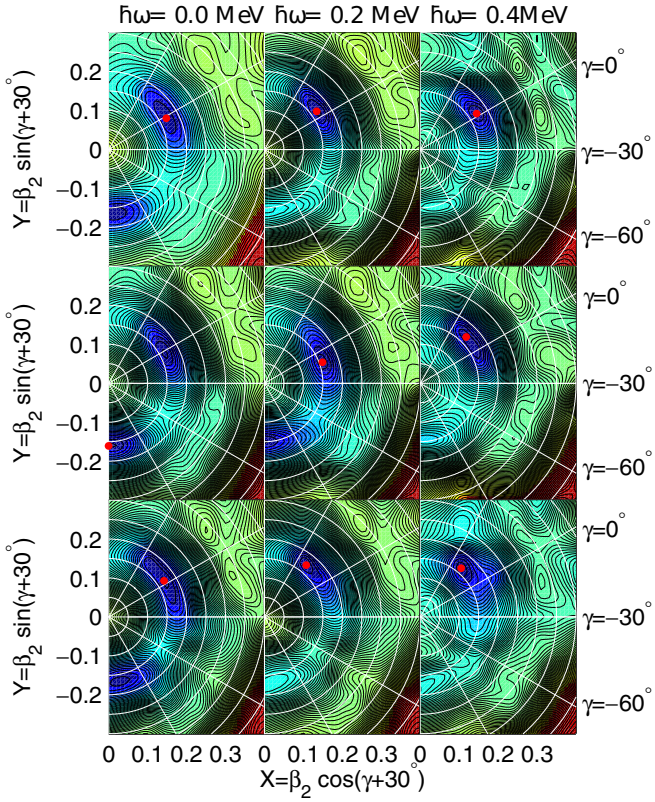

FIG. 4. (Color online) The TRS calculations for ^{166}Re at $\hbar\omega =$ 0.0, 0.2, and 0.4 MeV (left, middle, and right column, respectively) with the following proton and neutron (parity, signature) levels closest to the Fermi surface blocked: $\pi(-,-1/2)$ $\nu(+,+1/2)$, top row; $\pi(-,-1/2)$ $\nu(-,+1/2)$, middle row; and $\pi(+,-1/2)$ $\nu(+,+1/2)$, bottom row. The energy difference between successive contour curves is 100 keV. The solid circles in the figures denote the minima of the surfaces.

value $\gamma \approx 6^\circ$ to $\gamma \approx 0^\circ$ at $\hbar\omega \approx 0.30$ MeV. A prominent softness of the minimum in the γ degree of freedom should be noted. The nucleus remains in this axially symmetric shape until the maximum rotational frequency for which the band is observed, $\hbar\omega \approx 0.35$ MeV. For the yrare configurations (see the middle and bottom rows in Fig. 4) the β_2 deformation is similar to that of the yrast band. The triaxial parameter is similar, $\gamma \approx 8^\circ$, for the yrare (proton, $\pi = -, \alpha = -1/2$; neutron, $\pi = -, \alpha = +1/2$) configuration emanating from the $\pi h_{11/2} \otimes \nu h_{9/2}$ spherical state, while the lowest configuration emanating from the $\pi d_{5/2} \otimes \nu i_{13/2}$ spherical state exhibits a more stable near-triaxial shape with $\gamma \approx 21^\circ$. It should also be noted that the neutron $h_{9/2}$ state contains significant admixture from the $f_{7/2}$ subshell, as discussed below.

The structures of the two collective bands observed in ^{166}Re can be elucidated by considering aligned angular momenta, $B(M1)/B(E2)$ ratios, and signature splitting as a function of angular momentum or rotational frequency. Structural information can then be inferred by comparing with the properties of calculated configurations. With the β_2 deformation around 0.17 predicted by our TRS calculations, the Nilsson orbitals near the Fermi surface emanate from the $h_{11/2}$ and $d_{5/2}$ subshells for protons and are of $i_{13/2}$, $h_{9/2}$, and $f_{7/2}$ characters

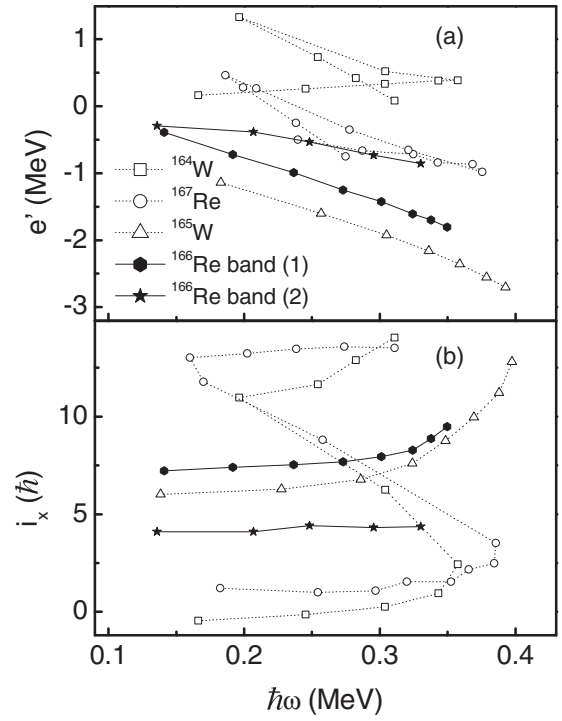

FIG. 5. Experimental quasiparticle (a) Routhians and (b) aligned angular momenta for bands (1) and (2) in ^{166}Re, as well as the systematic comparisons in ^{164,165}W [2,3] and ^{167}Re [31].

for neutrons. The yrast bands of ^{165}W and ^{167}Os are interpreted as built on the $\nu i_{13/2}[660]1/2^+$ configuration [3,30], while the yrast bands of the odd-N nuclei ^{167}Re and ^{169}Re are interpreted as based on the $\pi h_{11/2}[514]9/2^-$ configuration [8,31]. The $\pi h_{11/2}[514]9/2^- \otimes \nu i_{13/2}[660]1/2^+$ configuration is suggested for band (1) of ^{166}Re. Such an yrast configuration has also been assigned for ^{170,172}Re [8,9] and ^{164}Ta [6].

To test the quasiparticle configurations suggested for the rotational structures observed in ^{166}Re, the experimental Routhians and aligned angular momenta versus rotational frequency are shown in Fig. 5. The Harris parameters $\mathcal{J}_0 = 13\hbar^2$ MeV^{-1} and $\mathcal{J}_1 = 64\hbar^4$ MeV^{-3} were used for subtracting the contribution from the rotating core. From Fig. 5(b), one can see that $i_p \approx 1.3\hbar$ in ^{167}Re, $i_n \approx 6.3\hbar$ in ^{165}W, and the initial alignment in ^{166}Re is about 7.5 $\hbar$ at $\hbar\omega = 0.25$ MeV. The initial alignment in ^{166}Re is approximately the sum of the alignments from the odd-proton ^{167}Re and odd-neutron ^{165}W, which supports the configuration assignment for band (1) in ^{166}Re. Quasiparticle Routhians e' have been calculated with the universal Woods-Saxon potential [32,33]. The quasiparticles are labeled with the convention from Ref. [34] as shown in Table II; see Fig. 6. The neutron AB crossing is blocked in ^{166}Re owing to the occupation of the $\nu i_{13/2}[660]1/2^+$ orbital configuration. The aligned angular momentum plot shown in Fig. 5(b) reveals the beginning of an upbending at $\hbar\omega \approx 0.33$ MeV for band (1). This is consistent with the $i_{13/2}$ BC crossing frequency predicted by the cranked shell model (CSM) calculations at around 0.32 MeV shown in Fig. 6(a). The CSM prediction for the quasiproton crossing frequency is around 0.4 MeV, as shown in Fig. 6(b), i.e., somewhat later

TABLE II. The Nilsson labeling for quasiparticles in ^{166}Re, taken from Ref. [34].

Label	(π,α)	Nilsson configuration	Quasiparticle
A	$(+,+1/2)$	$i_{13/2}[660]1/2$	Neutrons
B	$(+,-1/2)$	$i_{13/2}[660]1/2$	Neutrons
C	$(+,+1/2)$	$i_{13/2}[651]3/2$	Neutrons
E	$(-,-1/2)$	$(f_{7/2}[532],h_{9/2}[521])3/2$	Neutrons
F	$(-,+1/2)$	$(f_{7/2}[532],h_{9/2}[521])3/2$	Neutrons
e	$(-,-1/2)$	$h_{11/2}[514]9/2$	Protons
f	$(-,+1/2)$	$h_{11/2}[514]9/2$	Protons

than the predicted BC crossing. The BC crossing has been observed in the yrast rotational bands of ^{170,172}Re [8,9], ^{162}Lu [35], and ^{162,164,166}Ta [5–7].

The configuration assignments are tested by considering the reduced transition probability $B(M1)/B(E2)$ ratios. A comparison between theoretical predictions within the Dönau-Frauendorf semiclassical approach and the experimentally deduced values is shown in Fig. 7. The experimental ratios

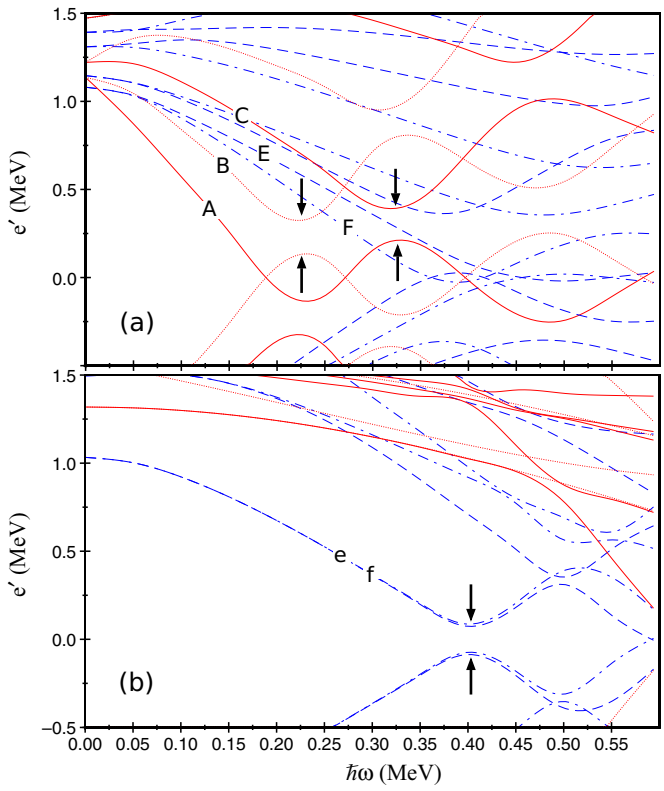

FIG. 6. (Color online) Cranked Routhians using the universal Woods-Saxon potential for (a) quasineutrons and (b) quasiprotons in ^{166}Re with the deformation parameters $\beta_2 = 0.17$, $\beta_4 = 0.009$, and $\gamma = -1.6^\circ$ from TRS predictions. Different lines represent different parity and signature (π,α): solid $(+,+1/2)$; dotted $(+,-1/2)$; dot-dashed $(-,+1/2)$; dashed $(-,-1/2)$. The labels for the configurations are given in Table II.

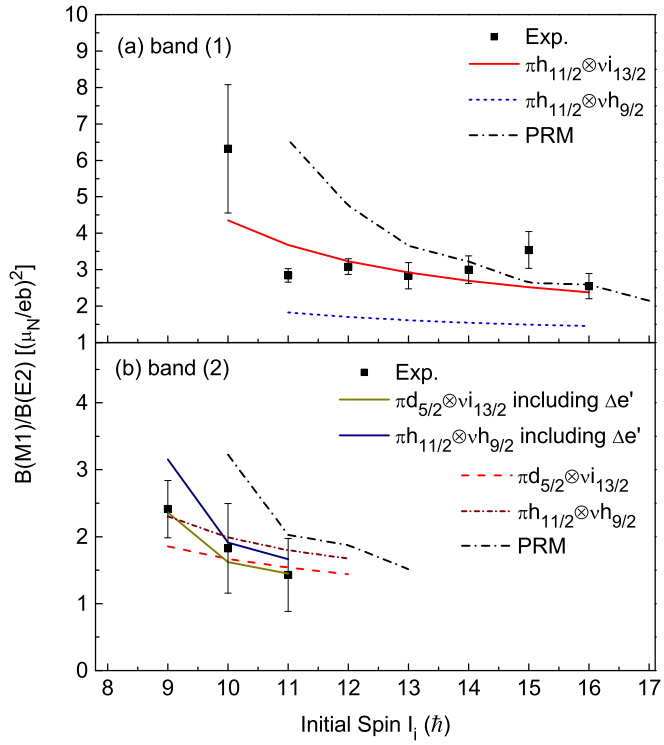

FIG. 7. (Color online) $B(M1)/B(E2)$ ratios for bands (1) and (2) in ^{166}Re. Experimental values are compared with theoretical predictions from semiclassical and particle-rotor model calculations. For band (2) the semiclassical calculations with and without the signature-dependent term in Eq. (3) are shown. See text for further details.

are extracted from the formula [36]

$$\frac{B(M1;I\to I-1)}{B(E2:I\to I-2)} = 0.697\frac{1}{\lambda}\frac{E_\gamma^5(E2)}{E_\gamma^3(M1)}\frac{1}{1+\delta^2}\left[\frac{\mu_N^2}{e^2b^2}\right], \tag{2}$$

where δ is the $E2$ admixture in the $M1$ transition and is set to zero in the calculation, λ is the $\Delta I = 2/\Delta I = 1$ branching ratios, and the energy is given in MeV. The branching ratios were deduced by gating on the transitions above the states of interest. The theoretical estimates of the $B(M1)/B(E2)$ values were derived using the Dönau-Frauendorf semiclassical model [37,38]:

$$\frac{B(M1;I\to I-1)}{B(E2;I\to I-2)} = \frac{12}{5Q_0^2\cos^2(\gamma+30^\circ)}\left[1-\frac{K^2}{(I-1/2)^2}\right]^{-2}\frac{K^2}{I^2} \times\left[(g_1-g_R)(\sqrt{I^2-K^2}-i_1)\left(1\pm\frac{\Delta e'}{\hbar\omega}\right)-(g_2-g_R)i_2\right]^2. \tag{3}$$

Here g_1 and i_1 are the g factor and alignment, respectively, for the deformation-aligned particle, while g_2 and i_2 correspond to rotation-aligned particles. The single-particle g factors were taken from Ref. [39] and the collective g factor g_R was

taken as Z/A. The quadrupole moment is given by $Q_0 = \frac{3}{\sqrt{5\pi}} R^2 Z\beta_2(1+0.16\beta_2)$, where the deformation parameters $\beta_2 \approx 0.17$ and $\gamma \approx 0^\circ$ were taken from the prediction of the TRS calculations and $R = 1.4A^{1/3}$ (fm). Figure 7(a) shows a fair agreement between the values deduced for band (1) and the theoretical prediction for the $\pi h_{11/2}[514]9/2^- \otimes \nu i_{13/2}[660]1/2^+$ configuration. The theoretical values for the yrare configuration emanating from the $\pi h_{11/2} \otimes \nu h_{9/2}$ spherical subshells are also shown as a comparison. Figure 7(b) shows the experimental $B(M1)/B(E2)$ ratios for band (2), as well as the theoretical predictions for different configurations near the Fermi surface. The signature-dependent term $(1 \pm \frac{\Delta e'}{\hbar\omega})$ is applied for band (2). Figure 7(b) shows that both the $\pi d_{5/2} \otimes \nu i_{13/2}$ and $\pi h_{11/2} \otimes \nu h_{9/2}$ configurations fit the experimental results. However, because the TRS calculations predict that the $\pi h_{11/2} \otimes \nu h_{9/2}$ configuration is more favored, we tentatively assign band (2) to this configuration.

Furthermore, particle-rotor model (PRM) calculations [40] have been performed to assign the configurations, as well as to study the signature splitting and signature inversion for bands (1) and (2), respectively. The Hamiltonian of the system is written as

$$H = \frac{\hbar^2}{2\theta} R^2 + \sum_{p,n}(H_{\rm sp} + H_{\rm pair}) + V_{pn}, \tag{4}$$

where the R describes the collective rotational angular momentum of an axially symmetric core, θ is moment of inertia, $H_{\rm sp}$ is the intrinsic single-particle energy in the deformed mean field of modified oscillator potential, $H_{\rm pair}$ is the monopole pairing interaction between like nucleons, and V_{pn} is the residual interaction between the valence proton and neutron. The κ, μ parameters of the deformed modified oscillator were taken from Ref. [41] and the variable moment of inertia (VMI) parameters are obtained from a least-squares fit to the level energies of the ground-state band in ^{164}W [2]. In the VMI description the decrease in energy spacing of the core with increasing spin, is regarded as a characteristic increase in the moment of inertia [42]. The residual interaction taken into account is of a spin-dependent δ-functional form,

$$V_{pn} = 4\pi\sqrt{\frac{\pi b^3}{\sqrt{2}}}\delta|\vec{r}_p - \vec{r}_n|(u_0 + u_1\vec{\sigma}_p.\vec{\sigma}_n), \tag{5}$$

where b is the oscillator length, and the strength parameters are defined as $u_0 = -4.95$ MeV and $u_1 = -0.55$ MeV [43] for both bands (1) and (2).

A comparison between the observed energy staggering $S(I)$ and the results of the PRM calculations is shown in Fig. 8. The staggering parameter $S(I)$ is defined as [9]

$$S(I) = E(I) - E(I-1) - \tfrac{1}{2}[E(I+1) - E(I) + E(I-1) - E(I-2)]. \tag{6}$$

From Fig. 8, it is apparent that the inclusion of the residual interaction V_{pn} plays an important role in successfully reproducing the signature splitting of the two-quasiparticle band (1). Additionally, the VMI description leads to the compression of the total energy staggering at higher spins in ^{166}Re, bringing it to excellent agreement with observed energy staggering for both bands (1) and (2).

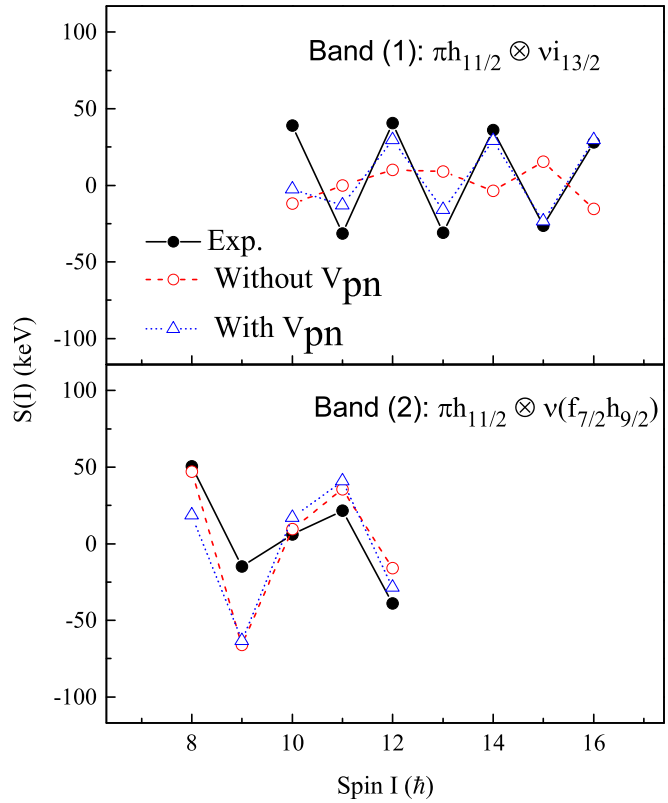

FIG. 8. (Color online) Calculated energy staggering using the PRM with and without residual interaction, as a function of spin I for bands (1) and (2) in ^{166}Re. Solid black circles represent the observed energy staggering.

The PRM calculations allow us to assign the $\pi h_{11/2}[514]9/2^- \otimes \nu i_{13/2}[660]1/2^+$ and mixed $\pi h_{11/2}[514]9/2^- \otimes \nu[f_{7/2}h_{9/2}]3/2^-$ Nilsson configurations for the positive and negative bands of ^{166}Re, respectively. With this assignment, the expected favored signature for band (1) should be even spins from the Gallagher-Moszkowski rule [44]. From Fig. 8, one can see that the expected favored signature is energetically higher than the unfavored one at the observed spins. However, the two signatures may reverse their phases at higher spins from the systematics in this $\pi h_{11/2} \otimes \nu i_{13/2}$ band [45]. The critical spin value for this abnormal signature inversion in ^{172}Re is 18.5$\hbar$ and there is an increasing trend of critical spin when the neutron number decreases [45]. Because the highest spin value identified for band (1) in the present work is 17$\hbar$, it might also be present in band (1) for ^{166}Re at higher values of angular momentum. The experimental staggering pattern for band (2) exhibits an abnormal signature inversion at the critical spin $I = 11\hbar$. Because the signature inversion is not sensitive to the V_{pn} interaction, its origin could be explained in terms of the mixing between $f_{7/2}$ and $h_{9/2}$ neutron levels, the latter becoming dominant at higher rotational frequencies. The underlying mechanisms behind the signature inversion phenomenon in general are still unclear. The present data on

^{166}Re may add important pieces to the puzzle as the signature inversion in band (2) is successfully explained by the mixing of neutron orbitals emanating from the $f_{7/2}$ and $h_{9/2}$ spherical subshells.

IV. SUMMARY

The level structure of ^{166}Re has been investigated via the ^{92}Mo(^{78}Kr, $3p1n$)^{166}Re reaction. Two collective band structures have been identified. The yrast band (1) has been assigned to the $\pi h_{11/2}[514]9/2^- \otimes \nu i_{13/2}[660]1/2^+$ Nilsson configuration based on rotational characteristics and electromagnetic properties in comparisons with Woods-Saxon mean-field, particle-rotor, and semiclassical calculations. The backbending observed in band (1) is interpreted as originating from the $i_{13/2}$ BC crossing. Alternative configuration assignments for band (2) have been investigated. For both the $\pi h_{11/2} \otimes \nu h_{9/2}$ and the $\pi d_{5/2} \otimes \nu i_{13/2}$ configurations, a fair agreement is obtained between the semiclassical calculations and the experimentally deduced $B(M1)/B(E2)$ ratios, while the TRS calculations favor the $\pi h_{11/2} \otimes \nu h_{9/2}$ configuration. Anomalous signature inversion is observed in band (2). The inversion and its critical spin is well reproduced by the PRM model calculations with the mixed $\pi h_{11/2}[514]9/2^- \otimes \nu[f_{7/2}h_{9/2}]3/2^-$ Nilsson configuration.

ACKNOWLEDGMENTS

The authors would like to thank the staff at the Accelerator Laboratory of the University of Jyväskylä for their excellent technical support. Enlightening discussions with I. Ragnarsson concerning the PRM calculations are gratefully acknowledged. This work was supported by the Swedish Research Council (Project No. 621-2010-3694), the Academy of Finland under the Finnish Centre of Excellence Programme 2012–2017, the UK Science and Technology Facilities Council, and theEuropean Union Seventh Framework Programme *Integrating Activities-Transnational Access*, Project No. 262010 (ENSAR). H.J.L. is supported in part by the China Scholarship Council under Grant No. 201306210205. Additionally, we thank the GAMMAPOOL European Spectroscopy Resource for the loan of the detectors for the JUROGAM II array. T.G. acknowledges the support from the Academy of Finland (Contract No. 131665).

[1] P. Möller, J. R. Nix, W. D. Myers, and W. J. Swiatecki, At. Data Nucl. Data Tables **59**, 185 (1995).
[2] J. Simpson, M. A. Riley, A. Alderson, M. A. Bentley, A. M. Bruce, D. M. Cullen, P. Fallon, F. Hanna, and L. Walker, J. Phys. G: Nucl. Part. Phys. **17**, 511 (1991).
[3] J. Simpson *et al.*, J. Phys. G: Nucl. Part. Phys. **18**, 1207 (1992).
[4] M. Sandzelius *et al.*, Phys. Rev. C **80**, 054316 (2009).
[5] F. Ghazi Moradi *et al.*, Phys. Rev. C **84**, 064312 (2011).
[6] D. G. Roux *et al.*, Phys. Rev. C **65**, 014308 (2001).
[7] D. J. Hartley *et al.*, Phys. Rev. C **82**, 057302 (2010).
[8] D. J. Hartley *et al.*, Phys. Rev. C **87**, 024315 (2013).
[9] Y. H. Zhang *et al.*, Phys. Rev. C **68**, 054313 (2003).
[10] Y. S. Chen, S. Frauendorf, and G. A. Leander, Phys. Rev. C **28**, 2437 (1983).
[11] R. Bengtsson, H. Frisk, R. F. May, and J. A. Pinston, Nucl. Phys. A **415**, 189 (1984).
[12] B. Cederwall *et al.*, Nucl. Phys. A **542**, 454 (1992).
[13] K.-H. Schmidt, R. S. Simon, J.-G. Keller, F. P. Hessberger, G. Münzenberg, B. Quint, H.-G. Clerc, W. Schwab, U. Gollerthan, and C.-C. Sahm, Phys. Lett. B **168**, 39 (1986).
[14] R. S. Simon, K.-H. Schmidt, F. P. Hessberger, S. Hlavac, M. Honusek, G. Münzenberg, H.-G. Clerc, U. Gollerthan, and W. Schwab, Z. Phys. A **325**, 197 (1986).
[15] B. Hadinia *et al.*, Phys. Rev. C **76**, 044312 (2007).
[16] M. J. Taylor *et al.*, Nucl. Instrum. Methods Phys. Res. A **707**, 143 (2013).
[17] C. W. Beausang *et al.*, Nucl. Instrum. Methods Phys. Res. A **313**, 37 (1992).
[18] C. Rossi Alvarez, Nucl. Phys. News **3**, 10 (1993).
[19] G. Duchêne, F. A. Beck, P. J. Twin, G. de France, D. Curien, L. Han, C. W. Beausang, M. A. Bentley, P. J. Nolan, and J. Simpson, Nucl. Instrum. Methods Phys. Res. A **432**, 90 (1999).
[20] M. Leino *et al.*, Nucl. Instrum. Methods Phys. Res. B **99**, 653 (1995).
[21] M. Leino, Nucl. Instrum. Methods Phys. Res. B **126**, 320 (1997).
[22] J. Sarén, J. Uusitalo, M. Leino, and J. Sorri, Nucl. Instrum. Methods Phys. Res. A **654**, 508 (2011).
[23] R. D. Page *et al.*, Nucl. Instrum. Methods Phys. Res. B **204**, 634 (2003).
[24] I. H. Lazarus *et al.*, IEEE Trans. Nucl. Sci. **48**, 567 (2001).
[25] P. Rahkila, Nucl. Instrum. Methods Phys. Res. A **595**, 637 (2008).
[26] D. C. Radford, Nucl. Instrum. Methods Phys. Res. A **361**, 297 (1995).
[27] H. J. Li *et al.*, Phys. Rev. C (to be published).
[28] W. Nazarewicz *et al.*, Nucl. Phys. A **503**, 285 (1989).
[29] W. Satula and R. Wyss, Phys. Scr., T **56**, 159 (1995).
[30] D. T. Joss *et al.*, Nucl. Phys. A **689**, 631 (2001).
[31] D. T. Joss *et al.*, Phys. Rev. C **68**, 014303 (2003).
[32] W. Nazarewicz, J. Dudek, R. Bengtsson, T. Bengtsson, and I. Ragnarsson, Nucl. Phys. A **435**, 397 (1985).
[33] S. Ćwiok, J. Dudek, W. Nazarewicz, J. Skalski, and T. Werner, Comput. Phys. Commun. **46**, 379 (1987).
[34] R. Wyss, J. Nyberg, A. Johnson, R. Bengtsson, and W. Nazarewicz, Phys. Lett. B **215**, 211 (1988).
[35] S. L. Gupta, S. C. Pancholi, P. Juneja, D. Mehta, A. Kumar, R. K. Bhowmik, S. Maralithar, G. Rodrigues, and R. P. Singh, Phys. Rev. C **56**, 1281 (1997).
[36] C. W. Beausang, L. Hildingsson, E. S. Paul, W. F. Piel, Jr., N. Xu, and D. B. Fossan, Phys. Rev. C **36**, 1810 (1987).
[37] F. Dönau and S. Frauendorf, in *Proceedings of the Conference on High Angular Momentum Properties of Nuclei, Oak Ridge*, edited by N. R. Johnson (Harwood, New York, 1983), p. 143.
[38] F. Dönau, Nucl. Phys. A **471**, 469 (1987).

[39] K. L. G. Heyde, in *The Nuclear Shell Model* (Springer-Verlag, Berlin Heidelberg, 1994), p. 174.
[40] I. Ragnarsson and P. B. Semmes, Hyperfine Interact. **43**, 425 (1988).
[41] T. Bengtsson and I. Ragnarsson, Nucl. Phys. A **436**, 14 (1985).
[42] M. A. J. Mariscotti, G. S. Goldhaber, and B. Buck, Phys. Rev. **178**, 1864 (1969).
[43] W. Reviol *et al.*, Phys. Rev. C **59**, 1351 (1999).
[44] C. J. Gallagher, Jr., and S. A. Moszkowski, Phys. Rev. **111**, 1282 (1958).
[45] Y. H. Zhang *et al.*, Chin. Phys. Lett. **22**, 2788 (2005).